PERGAMON

International Journal of Multiphase Flow 27 (2001) 753–763

International Journal of Multiphase Flow

www.elsevier.com/locate/ijmulflow

Merging of drops to form bamboo waves

Yuriko Y. Renardy *, Jie Li

Department of Mathematics, Virginia Polytechnic Institute and State University, Blacksburg, VA 24061-0123, USA

Received 17 January 2000; received in revised form 23 September 2000

Abstract

Topological transitions in core-annular flow of oil and water are described. Drops of one liquid are suspended in the second liquid and transported through a pipeline under a pressure gradient. We examine the merging of an array of drops in this two-fluid flow. Larger drops are found to merge and the flow undergoes a topological transition to core-annular flow. In core-annular flow of two liquids, one liquid lies at the core and the other surrounds it. For the case of large oil bubbles in water, a steady core-annular flow with bamboo waves on the interface is achieved. For the case of large water bubbles in oil, the ensuing core-annular flow has continually breaking waves at the interface.

Keywords: Core-annular flow; Bamboo waves; Direct numerical simulation; Volume-of-fluid scheme

1. Introduction

Two-phase flows of oil and water can have different flow types depending on the flow rates. The flow types shown in Figs. 2–5 of Joseph et al. (1997) and Chapters V and VII of Joseph and Renardy (1993) for vertical pressure-driven flow include perfect core-annular flow, wavy core-annular flow, slugs of oil in water, and drops of oil in water, and drops of water in oil. Figure 3.4 (b) of Joseph and Renardy (1993) shows drops of a heavy Mobil oil in water, in both upflow where gravity opposes the applied pressure gradient, and downflow where gravity aids the applied pressure gradient. Figure 15.1 of Joseph and Renardy (1993) shows oil bubbles in water. A comprehensive classification of flow types for the case of matched density (oil plus additive in water) was given by Charles et al. (1961). Their Fig. 4 also shows the previously mentioned flow types, including water drops in oil, and oil drops in water. The flow types are correlated with prescribed input data. Typically, superficial velocities are given for the flows. The superficial velocity is $U_o = Q_o/A$ for oil and $U_w = Q_w/A$ for water, where Q_o and Q_w are the volume flow

* Corresponding author. Fax: +1-540-231-5960.

0301-9322/01/$ - see front matter
PII: S0301-9322(00)00058-6

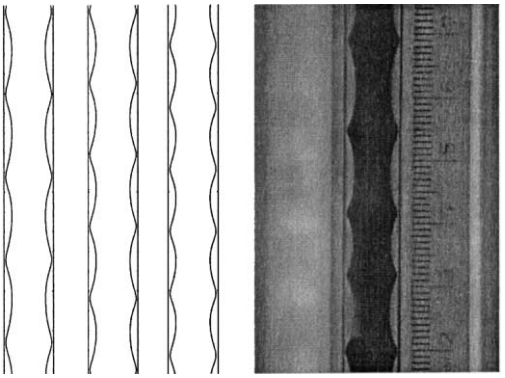

Fig. 1. Up-flow for $Re = 0.93$, $a = 1.28$, $m = 0.00166$, $\zeta = 1.1$, $J = 0.0795$ and $K = -0.4552$. The photograph on the right is experimentally obtained. Our numerical simulations are on the left, for dimensionless wavenumbers $\alpha = 1.5, 1.75, 2.0$.

rates of oil and water, and $A = \pi R_2^2$ is the cross-sectional area of the pipe. Flow charts delineate regions in the plane of superficial velocities. In experiments in the vertical inverted loop of Bai et al. (1992), the oil is lighter than water so that buoyancy and the pressure gradient act in the same sense in up-flow, where the core is stretched to produce bamboo waves over a wide interval of superficial velocities. For slower oil speeds, slugs and bubbles of oil in water occur, while at faster oil speeds, water drops form in oil. The bamboo waves are a robust regime, and have been simulated numerically in Li and Renardy (1999): the initial condition was composed of perfect core-annular flow together with a large-amplitude perturbation in the form of an axisymmetric eigenfunction. The time-dependent axisymmetric simulation of this initial condition was found to settle to the bamboo wave solution, as shown in Fig. 1. The parameters in the figure caption are defined in Section 3. In this paper, we shall see that the bamboo wave solution can also be achieved with other initial conditions, such as a string of drops of oil in water.

2. Numerical method

There are many interface tracking methods, such as the moving grid method, the front tracking method, the level set method and the volume-of-fluid (VOF) method. The VOF method provides a simple way of treating the topological changes of the interface. A recent review article is that of Scardovelli and Zaleski (1999) and we refer the reader to the references therein. Our code SURFER++ is composed of three parts: a second-order VOF method to track the interface, a projection method to solve the Navier–Stokes equations on the MAC grid, and finally, a continuum method for modeling the interfacial tension. We describe these components below.

2.1. Governing equations

The density ρ and the viscosity μ of each fluid is a constant in each fluid but we allow for the possibility of a jump across the interface. A concentration (or color) function C is used to represent and track the interface:

$$C(\boldsymbol{x}) = \begin{cases} 1 & \text{fluid 1,} \\ 0 & \text{fluid 2.} \end{cases}$$

This concentration function is transported by the velocity field $\boldsymbol{u}$. The average values of the density and the viscosity are given by $\rho = C\rho_1 + (1-C)\rho_2$ and $\mu = C\mu_1 + (1-C)\mu_2$, where subscripts refer to fluids 1 and 2. We suppose also that the flow is incompressible: $\nabla \cdot \boldsymbol{u} = 0$, and governed by the Navier–Stokes equation:

$$\rho\left(\frac{\partial \boldsymbol{u}}{\partial t} + \boldsymbol{u} \cdot \nabla \boldsymbol{u}\right) = -\nabla p + \nabla \cdot \mu \boldsymbol{S} + \boldsymbol{F},$$

where $\boldsymbol{S}$ is the viscous stress tensor:

$$\boldsymbol{S}_{ij} = \left(\frac{\partial u_j}{\partial x_i} + \frac{\partial u_i}{\partial x_j}\right).$$

The body force $\boldsymbol{F}$ includes the gravity and interfacial tension force. The interfacial tension force is $\boldsymbol{F}_{\mathrm{s}} = \sigma\kappa\boldsymbol{n}_{\mathrm{S}}\delta_{\mathrm{S}}$, where σ is the interfacial tension, κ the mean curvature and $\boldsymbol{n}_{\mathrm{S}}$ is the normal to the interface.

2.2. Temporal discretization and projection method

The simultaneous solution of the large system which arises from discretizing the governing equations is very costly, especially in three spatial dimensions. An efficient approximation can be obtained by decoupling the solution of the Navier–Stokes equations from the solution of the continuity equation by a projection method.

The pressure is decomposed into two parts, $-fx + p$, where f is the driving pressure gradient. In the projection method, the momentum equations are first solved for an approximate $\boldsymbol{u}^*$ assuming that $\boldsymbol{u}^n$ is known

$$\frac{\boldsymbol{u}^* - \boldsymbol{u}^n}{\Delta t} = -\boldsymbol{u}^n \cdot \nabla \boldsymbol{u}^n + \frac{1}{\rho}(\boldsymbol{f} + \nabla \cdot (\mu \boldsymbol{S}) + \boldsymbol{F} + \rho \boldsymbol{g})^n,$$

where the driving pressure gradient $\boldsymbol{f}$ is treated as a body force. In general, the intermediate flow field $\boldsymbol{u}^*$ does not satisfy the incompressibility equation. It is corrected by the pressure

$$\frac{\boldsymbol{u}^{n+1} - \boldsymbol{u}^*}{\Delta t} = -\frac{\nabla p}{\rho},$$

in order to yield a divergence free velocity $\boldsymbol{u}^{n+1}$ at the next time step. The pressure field is not known in this equation, but by taking the divergence of this equation, it is found to satisfy Poisson equation,

$$\nabla \cdot \left(\frac{\nabla p}{\rho}\right) = \frac{\nabla \cdot \boldsymbol{u}^*}{\Delta t}.$$

In the problems we address below, the boundary conditions for the velocity are periodicity and the Dirichlet condition. Analogously, the boundary conditions for the pressure are periodicity and the Neumann condition, respectively.

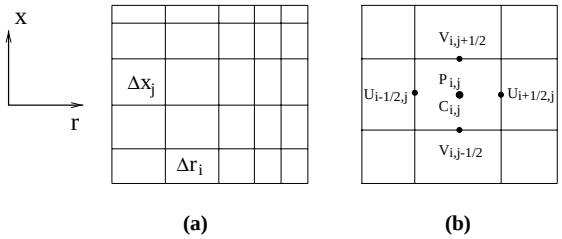

Fig. 2. (a) Two-dimensional Cartesian mesh with variable cell sizes; (b) Location of variables in an MAC mesh cell.

2.3. Spatial discretization

The spatial discretization of the momentum equation and Poisson equation for the pressure is based on a finite difference scheme known as the MAC method. A mesh of rectangular cells is used, with variable sizes, as shown in Fig. 2. The gridpoints for the pressures and velocities differ: while the pressure and the concentration function C are given at nodes in the center of each rectangular cell, the velocities are given at the centers of the faces as indicated in Fig. 2.

2.4. Advection of the interface

At the discrete level, the concentration function is the volume fraction field C_{ij}: when a cell is filled by the fluid 1, $C_{ij} = 1$; when a cell does not contain any of this fluid, $C_{ij} = 0$. The interfaces are in the cells with C_{ij} between 0 and 1. When we represent the interface by a volume fraction field, we lose interface information and we cannot determine a unique interface; the interface must be reconstructed. We use the piecewise linear interface calculation (PLIC) method. The gist is to calculate the approximate normal $\boldsymbol{n}$ to the interface in each cell, since this determines one unique linear interface with the volume fraction of the cell. The discrete gradient of the volume fraction field yields: $\boldsymbol{n} = \nabla^h C/(|\nabla^h C|)$.

The second step of the VOF method is to evolve the volume fraction field C. Lagrangian method is the natural choice for interface evolution. In this scheme, once the interface is reconstructed, the velocity at the interface is interpolated linearly and then the new interface position is calculated via $\boldsymbol{x}^{n+1} = \boldsymbol{x}^n + \boldsymbol{u}(\Delta t)$. Fig. 3 illustrates how Lagrangian method performs on an arbitrary two-dimensional mesh. In comparison with Eulerian method, Lagrangian method has the following advantages: when the Courant condition $(\mathrm{Max}|\boldsymbol{u}|)\Delta t/h < 1/2$ is satisfied, this method is stable, and the volume fraction always satisfies the physical constraint $0 \leqslant C \leqslant 1$.

In the VOF method, the interfacial tension condition across the interface is not applied directly, but rather as a body force over the cells which contain the interface. Two such formulations have been implemented in this work. The first is the continuous surface force formulation, in which $\boldsymbol{f}_s = \sigma\kappa\boldsymbol{n}_S$ and $\boldsymbol{F}_s = \boldsymbol{f}_s\nabla C$. The second is the continuous surface stress formulation, in which $\boldsymbol{F}_s = \nabla \cdot \boldsymbol{T} = \sigma\delta_S\kappa\boldsymbol{n}_S$ and $\boldsymbol{T} = [(\boldsymbol{1} - \boldsymbol{n}_S \otimes \boldsymbol{n}_S)\sigma\delta_S]$, which leads to a conservative scheme for the momentum equation. Their performances are similar.

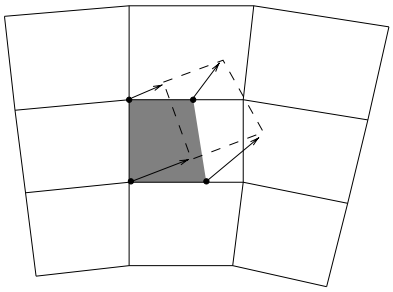

Fig. 3. Lagrangian method on arbitrary two-dimensional mesh. Shaded polygon represents part occupied by the fluid in the central cell. Broken line shows the polygon position after advection in the local velocity field represented by arrows. The fluid is redistributed between neighboring cells which the new polygon partially overlaps.

2.5. Semi-implicit stokes solver

The above is an explicit method, and not suitable for simulations at low Reynolds numbers that occur in the oil. For an explicit method, the time step Δt should be less than the viscous time scale, $T_\mu = \rho h^2/\mu$, where h denotes the mesh size. This stability limit is much more restrictive than the CFL condition for simulations of low Reynolds number flows. In order to carry out calculations for times of order 1, the implicit treatment of the viscous terms has been developed and is described in Li and Renardy (1999). The time integration scheme is constructed to be implicit for the Stokes operator and otherwise explicit. In summary, this scheme is first-order accurate and unconditionally stable. The stability of this scheme is crucial for simulation of low Reynolds number flow in the oil.

3. Flow parameters

We consider vertical pipeline transportation of two liquids driven by a pressure gradient. As shown in Fig. 4, liquid 1 is the drop liquid and liquid 2 is the surrounding liquid. In dimensional terms, the pipe radius is denoted L_x, the computational length in the axial direction L_y, T the interfacial tension, and the pressure gradient in the axial direction is a constant: $\mathrm{d}P^*/\mathrm{d}x = -f^*$. Initially, the drop is an ellipsoid of radii a_x and a_y, centered at (c_x, c_y). The simulation of large drops can lead to merging and formation of a disturbed core-annular flow called bamboo waves shown in Fig. 1, and we therefore, relate our parameters to those of core-annular flow. In core-annular flow, the notation used in Li and Renardy (1999) is as follows: the dimensional pipe radius is R_2 and the undisturbed radius of the core is R_1. In our drop problem, the volume of the initial ellipsoidal drop is $(4/3)\pi a_x^2 a_y$, and the volume of the computational domain is $\pi L_x^2 L_y$. The corresponding core-annular flow with the same volume ratio of the core to annular liquids as the drop simulation work with drop to outer liquids yields: $R_2 = L_x$ and $R_1^2/R_2^2 = (4/3)a_x^2 a_y/(L_x^2 L_y)$

$$R_1 = \frac{2a_x}{\sqrt{3}}\sqrt{\frac{a_y}{L_y}}.$$

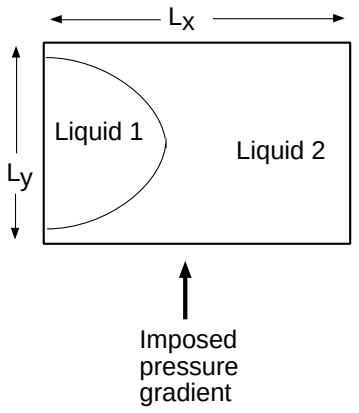

Fig. 4. Axisymmetric flow computational domain, periodic in the y direction with period $L_y = 2\pi/\alpha$. The pipe radius is L_x.

These expressions allow us to non-dimensionalize the drop problem in a manner which is consistent with core-annular flow. Dimensionless variables are chosen to be $(r,x) = (r^*,x^*)/R_1$, $(u,v) = (u^*,v^*)/V_0^*(0)$, $t = t^*V_0^*(0)/R_1$, $P = P^*/[\rho_1 V_0^{*2}(0)]$, where $V_0^*(0)$ denotes the centerline velocity in the corresponding core-annular flow:

$$V_0^*(0) = (f^* + \rho_2 g)\frac{R_1^2}{4\mu_2}A, A = mK + a^2 - 1 + 2(K-1)\log\ a.$$

The following are the six dimensionless parameters: the viscosity ratio $m = \mu_2/\mu_1$, length ratio $a = R_2/R_1$, density ratio $\zeta = \rho_2/\rho_1$, ratio of driving forces $K = (f^* + \rho_1 g)/(f^* + \rho_2 g)$, Reynolds number $Re = \rho_1 V_0^*(0)R_1/\mu_1$, and interfacial tension parameter $J = T^*R_1\rho_1/\mu_1^2$. These are related to the parameters used by Bai et al. (1992) via $J = J^*/a$ and $K = (1+F)/(\zeta+F)$, where $F = f^*/(\rho_1 g)$.

4. Numerical results

We consider a periodic array of drops in vertical pipe flow as in Fig. 4. We choose flow parameters that reflect the conditions under which bamboo waves such as Fig. 1 are observed. The oil density is 0.905 g cm^{-3}, oil viscosity is 6.01 poise, water density is 0.995 g cm^{-3} and water viscosity is 0.01 poise, $R_2 = 3/16$ inch $= 0.47625$ cm, $T^* = 8.54$ dyn/cm, $J^* = \rho_o T^* R_2/\mu_o^2 = 0.102$.

The computational domain for this axisymmetric flow is shown in Fig. 4 with $L_x = 1.28$ and $L_y = \pi$. The figures are drawn with three of the periodic array of cells over the vertical cross-section of the pipe. The density ratio is $\zeta = 1.1$ and the viscosity ratio is $m = 0.00166$.

In Fig. 5, $K = -0.9993$ as in the core-annular flows simulated in Figs. 9–11 of Li and Renardy (1999). The initial drop has its center at $(0,\pi/2)$ and the radii are 0.9 and 1.3 in the x and y directions, respectively. The mesh is 64×256. The oil drops first rise and then flatten and then begin to fall. The pressure gradient drives the central oil drops upward, while the heavier water is driven down by gravity counteracting the pressure gradient. In perfect core-annular flow, where

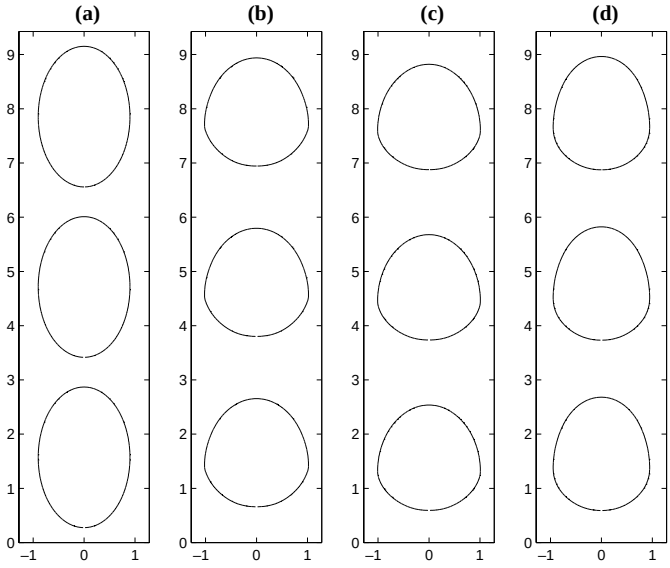

Fig. 5. Oil drops in water; interface positions at 1 s, 41 s, 81 s, 121 s.

most of the volume is oil, water is dragged along with the core oil. In this bubble flow, most of the volume is water, and hence the oil is dragged down by the water. A steady-state is achieved where the shape is flatter at the bottom. This shape is observed in the photograph of up-flow in Figure 3.4(b) of Joseph and Renardy (1993).

In Fig. 6, the drops are water and the outer liquid is oil. The initial ellipsoidal radii are $a_x = 0.5, a_y = 1.0$. In order to push the water drops upwards, the driving pressure gradient is

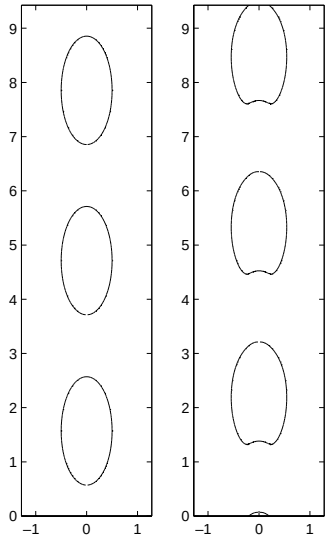

Fig. 6. Water drops in oil; 0 s, 125 s.

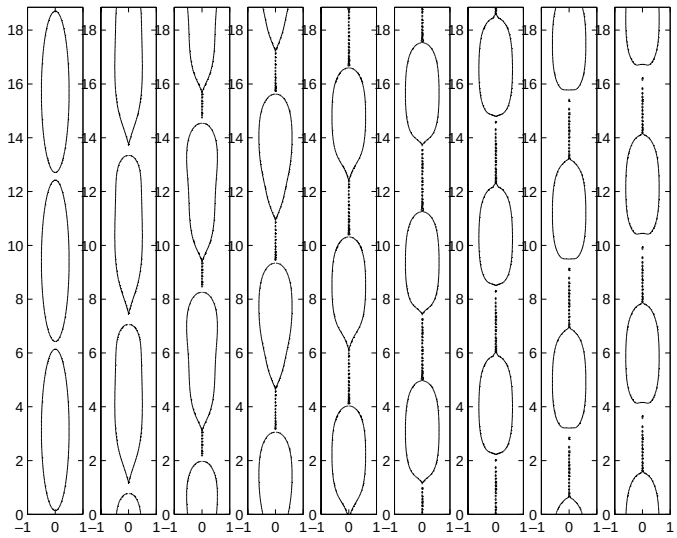

Fig. 7. Water drops in oil; 0 s, 10 s, 20 s, 30 s, 40 s, 50 s, 60 s, 70 s, 80 s.

increased by a factor 1.5 from that of Fig. 5. The water drops attain a steady-state shape with a dimple at the bottom and smooth rounded top, which is a distinctly different shape from the oil drops.

Longer drops are examined under the same pressure gradient in Fig. 7, where the computational domain is $1 \times 2\pi$. The initial ellipsoid is centered at $(0, \pi)$ with radii $a_x = 0.5, a_y = 3.0$. The drops reach a steady-state shape, translating upwards, with a dimple at the bottom of the drops and a filament extending out at the top. The drops or filaments are on the order of the mesh size and require mesh refinement to resolve the features. However, the shapes are those of the slugs observed in pipe flow.

Larger drops of oil evolve to shapes which approach the pipe walls. Since our code does not deal with contact lines, results will be shown only for evolutions that do not touch the walls. Fig. 8 shows evolution to bell-shaped drops. The mesh has been refined to 64×512. The center of the drop is as before. The radii are 1.2 and 1.55 in the x and y directions. The driving pressure gradient is as in the previous figure. With a slightly smaller initial drop (radii 1.15 and 1.55 in the x and y directions) but the driving pressure gradient increased by a factor 1.5, the drops assume even more of the bell shapes, as shown in Fig. 9.

Fig. 10 shows the evolution of drops on a 64×512 mesh, with the driving pressure gradient of the bamboo waves treated in Li and Renardy (1999), as in Figs. 5–8. The radii of the initial drop are 1.2 and 1.55 in the x and y directions. The interfacial tension has been decreased by a factor of 2.66. The drops merge and eventually saturate to large amplitude bamboo waves. Lower amplitude bamboo waves such as those simulated in Fig. 1 (cf. Li and Renardy, 1999) have symmetric crests. At larger amplitudes, a slight asymmetry sets in.

The liquids are exchanged in Fig. 11, where the drop liquid is now water and the outer liquid is oil. The driving pressure gradient of Fig. 10 did not move the water drops, which occupy most of the domain and are heavier than the oil. Rather, the water drops evolved to steady-state apple-like

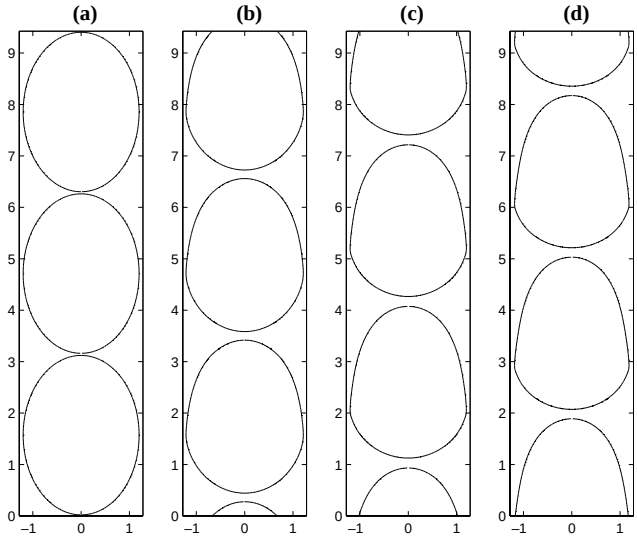

Fig. 8. Oil drops in water; interface positions at 0 s, 19 s, 38 s, 57 s.

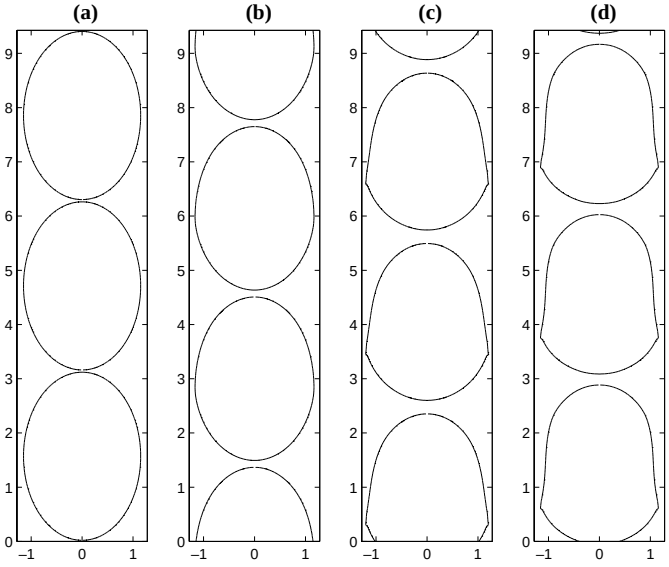

Fig. 9. Oil drops in water; interface positions at 0 s, 6.5 s, 13 s, 19.5 s. 64×512 mesh.

shapes. The driving pressure gradient was increased by a factor 1.5 to the same level as Fig. 9, and this is sufficient to push the water drops upwards. These first evolve to apple-like shapes, and then merge and form a core-annular flow, where the interface develops fins. This evolution is distinct from the case of oil drops in that the interfacial waves are breaking waves and do not reach a steady-state.

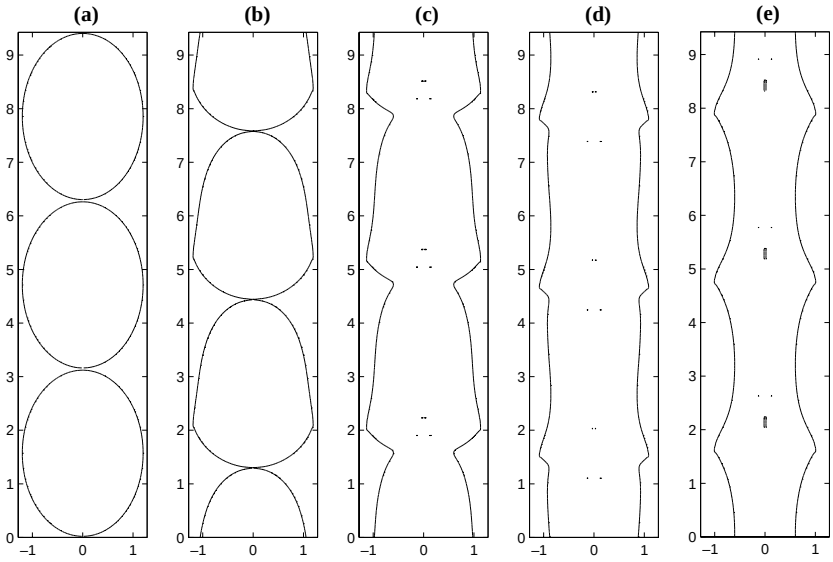

Fig. 10. Oil drops in water; interface shapes at 0 s, 40 s, 80 s, 120 s, 418 s. 64×512 mesh.

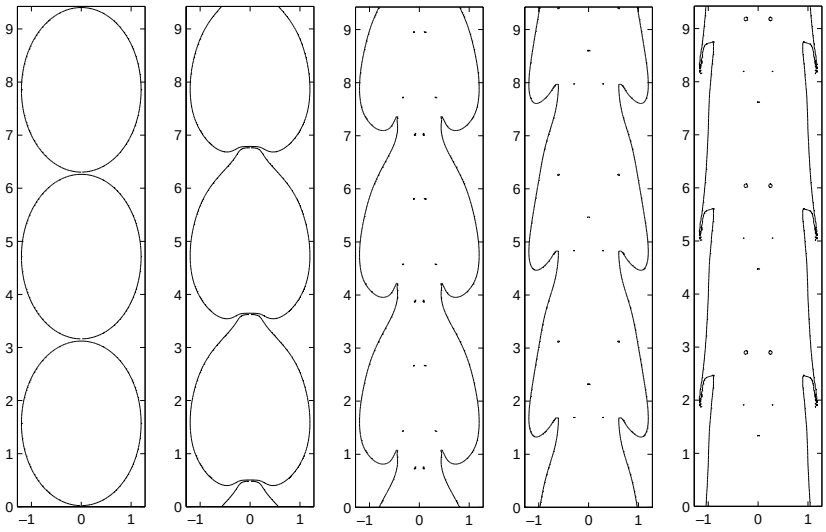

Fig. 11. Water drops in oil; 0 s, 3 s, 6.14 s, 12.39 s, 29.04 s.

5. Conclusion

We have examined the evolution of a periodic array of drops in two-fluid flow of oil and water, driven by a pressure gradient. When the oil drops are small, they evolve into disc or bell shapes. If they are closely packed, they may form bamboo waves. If the oil drops are large and the flow is fast, then they touch the walls. When the liquids are reversed, the water drops in oil evolve to

oblong shapes with a dimple at the bottom, and possibly filaments. When water drops merge to form core-annular flow, the interface evolves to continually breaking waves. These trends are consistent with the flow chart of Joseph and Renardy (1993) Figure 16.1. The types of flow that arise in up-flow include the transition of oil slugs to oil sticking to the wall, and transition of oil slugs to bamboo or disturbed bamboo waves.

Acknowledgements

This research was sponsored by the National Science Foundation under Grant CTS-9612308, INT-9815106 and ACS-PRF. We thank Stephane Zaleski for the use of the code SURFER. This work was supported by NCSA under Grants CTS990010N, CTS990059N, and CTS990063N.

References

Bai, R., Chen, K., Joseph, D.D., 1992. Lubricated pipelining: stability of core-annular flow part. 5. Experiments and comparison with theory. J. Fluid Mech. 240, 97–142.

Charles, M.E., Govier, G.W., Hodgson, G.W., 1961. The horizontal pipeline flow of equal density oil–water mixtures. Can. J. Chem. Eng. 39, 17.

Joseph, D.D., Bai, R., Chen, K., Renardy, Y.Y., 1997. Core-annular flows. Ann. Rev. Fluid Mech. 29, 65–90.

Joseph, D.D., Renardy, Y.Y., 1993. Fundamentals of Two-Fluid Dynamics Part. Springer, Berlin.

Li, J., Renardy, Y., 1999. Direct simulation of unsteady axisymmetric core-annular flow with high viscosity ratio. J. Fluid Mech. 391, 123–149.

Scardovelli, R., Zaleski, S., 1999. Direct numerical simulation of free surface and interfacial flow. Ann. Rev. Fluid Mech. 31, 567–604.